Lamellar phases confined in quasicylindrical pores: Lattice model results

M. Tasinkevych,[1] A. Ciach,[2] and M. M. Telo da Gama[1]
[1] *Departamento de Física da Faculdade de Ciências and Centro de Física Teórica e Computacional, Universidade de Lisboa, Avenida Professor Gama Pinto 2, P-1649-003 Lisboa Codex, Portugal*
[2] *Institute of Physical Chemistry, Polish Academy of Sciences, 01-224 Warsaw, Poland*
(Received 25 September 2001; published 12 February 2002)

A two-dimensional (2D) vector lattice model of microemulsions is applied to study the structure of lamellar phases confined in long rectangular pores. One-point distribution functions are calculated within mean field approximation. The effects of pore geometry and surface fields are considered. A 2D analog of an onion phase is favored by a pore with strongly hydrophilic walls. For neutral walls, far from the phase boundaries, the lamellar phase is stable inside the pore. By contrast, close to the lamellar-tubular phase boundary a pore with neutral walls favors a 2D tubular phase. This is the analog of capillary condensation. In all cases the excess pressure is calculated as a function of the pore geometry.

DOI: 10.1103/PhysRevE.65.031707 PACS number(s): 83.80.Xz, 68.15.+e, 68.55.Jk, 68.60.−p

I. INTRODUCTION

Amphiphilic molecules (surfactants, lipids, or block copolymers) consist of two distinct groups that differ significantly in their solubility. For instance, the hydrophilic head of a surfactant molecule prefers to dissolve in water, whereas the hydrophobic tail prefers to dissolve in oil. Consequently, in mixtures with water and oil, surfactant molecules self-assemble into monolayers that form a rich variety of mesostructures [1–3]. Spontaneous structure formation may be relevant technologically, for example, in the manufacture of very small devices. However, in small systems self-assembly is influenced significantly by the geometry, chemistry, and the size of the confining walls. Confinement plays a major role when the size of the system is comparable to the length characterizing the structure of the confined fluid. In microemulsions and lamellar phases the typical length λ corresponds to the size of correlated domains (for example, the size of micelles or the period of lamellar phases) and may be up to two orders of magnitude larger than molecular dimensions. Finite size effects are thus expected to occur on mesoscopic scales.

In lamellar phases, that consist of oil- and water-rich layers (lamellas) separated by monolayers of the surfactant, the translational and rotational symmetries are broken. Thus, the geometry of the confining walls may have significant effects on the self-assembly of these structures. In this work we consider a pore modeled by a box $L_x \times L_y \times L_z$. Previous theoretical studies [4–8] were restricted to slit geometries, i.e., to $L_y, L_z \to \infty$ with finite L_x. A capillarylike or quasicylindrical pore corresponds to $L_z \to \infty$ with both L_x and L_y finite. The structural and mechanical properties of lamellar phases confined in quasicylindrical pores with a base of size $\sim 10\lambda$ may be significantly different from those of lamellar phases confined in slits of similar widths, under the same thermodynamic conditions. In slits with strongly hydrophilic walls the lamellas are expected to be parallel to the walls. Theory [4,6,8] and experiment [9,10] confirm this. By contrast, for long square base pores with hydrophilic walls, one pair of (parallel) walls favors an orientation of the lamellas at right angles to the orientation favored by the other pair. Neither the structure nor the mechanical properties of confined lamellar phases are easily predicted in this case. Therefore, results based on simple model systems will give valuable insights and will help to interpret the results of future experiments.

In previous works [4–6] the effects of the confinement on the structural and mechanical properties of ternary surfactant mixtures in slitlike pores have been studied within the lattice Ciach-Høye-Stell (CHS) model [11]. The results [4] are in good agreement with experiments [10]. Since the CHS model has been proved useful in the analysis of self-assembly into various simple structures [4–6], we will extend it here to more complex confining geometries, such as quasicylindrical pores.

The thermodynamic and mechanical properties of confined lamellar phases are summarized in the following section. The model is described briefly in Sec. III., and the results are presented in Sec. IV. The final section contains a summary and discussion.

II. PHENOMENOLOGY

We start with a brief description of the thermodynamic properties of a system confined in a box. We assume that the system is in equilibrium with a reservoir, and that the temperature T and the chemical potentials μ_i are fixed. For a system with identical parallel walls, the variation in the grand termodynamic potential can be written as

$$\begin{aligned} d\Omega = {} & \omega_b d(L_x L_y L_z) + 2\sigma_x d(L_y L_z) + 2\sigma_y d(L_x L_z) \\ & + 2\sigma_z d(L_x L_y) + f_x L_y L_z dL_x + f_y L_x L_z dL_y \\ & + f_z L_x L_y dL_z, \end{aligned} \tag{1}$$

where ω_b is the bulk thermodynamic potential density, σ_x, σ_y and σ_z are the wall-fluid surface tensions for walls perpendicular to $\hat{\mathbf{x}}$, $\hat{\mathbf{y}}$, and $\hat{\mathbf{z}}$ respectively, while f_x, f_y, and f_z are related to the excess pressure in the direction denoted by the subscripts. For fixed $L_z \gg L_x, L_y$, the above simplifies to

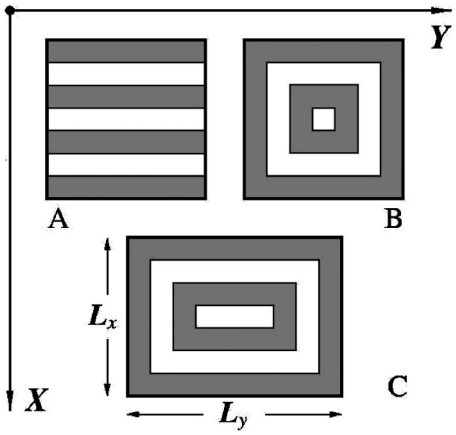

FIG. 1. Schematic representation of the structures formed by the lamellar phase in a long pore with a square or rectangular base. A cross section $z=\text{const}$ is shown for (a) lamellas parallel to one pair of walls, (b) quasionion structure for $L_x=L_y$, (c) quasionion structure for $L_x<L_y$.

$$d\Omega/L_z=\omega_b d(L_xL_y)+2\sigma_x dL_y+2\sigma_y dL_x+f_xL_y dL_x + f_yL_x dL_y. \tag{2}$$

The excess pressure in the x direction is defined as

$$\Pi_x=-\left(\frac{\partial\Omega_{ex}}{\partial V}\right)_{L_y,L_z}=-\frac{1}{L_yL_z}\left(\frac{\partial\Omega_{ex}}{\partial L_x}\right), \tag{3}$$

where V is the volume, and the excess grand thermodynamic potential of the system confined in the box is

$$\Omega_{ex}=\Omega-\omega_bL_xL_yL_z. \tag{4}$$

Π_y is defined in a similar way. For a square base pore, $L_x=L_y=L$, symmetry conserving compressions or expansions are associated with an excess pressure given by

$$\Pi=-\left(\frac{\partial\Omega_{ex}}{\partial V}\right)_{L_z}=-\frac{1}{2L_zL}\left(\frac{\partial\Omega_{ex}}{\partial L}\right). \tag{5}$$

Ω_{ex}, and consequently the excess pressure, depend significantly on the structure of the confined fluid. Different boundary conditions may lead to the stability or metastability of different structures. As we are not capable of determining, *a priori*, the stable structure under a particular set of conditions, we will consider the properties of the confined lamellar phases in a number of different structures, shown in Fig. 1.

A. Lamellar structure

The structure shown in Fig. 1(a) exhibits lamellas parallel to one pair of walls, and was studied in Ref. [4] for slit geometries, $L_y,L_z\to\infty$. For wide slits, $L_x\gg\lambda$, with N lamellas, the excess grand potential Ω_{ex} contains an elastic contribution $\Omega_{el}(L_x)/L_yL_z=B_l(L_x-L_N)^2/2L_N$, where B_l is the modulus of elasticity, L_N is the width of the slit under zero stress. $L_N^t<L_x<L_{N+1}^t$, with L_N^t the width of the slit where the transition from $N-1$ to N confined layers occurs. For $N\gg1$, $L_N^t\approx L_N-\lambda/2$, with λ the period of the bulk lamellar phase. The period of the lamellar phase in the slit is different from λ, except when $L_x=L_N$; thus, $L_{N+1}-L_N=\lambda$. We assume that for finite $L_y=\text{const}$, the elastic contribution to Ω is similar to that for a slit. Then considering lamellas parallel to the (y,z) wall, we write

$$\Omega_{ex}/L_yL_z\approx2\sigma_\parallel+2\sigma_\perp\frac{L_x}{L_y}+\frac{B_l(L_x-L_N)^2}{2L_N} \qquad (L_N^t<L_x<L_{N+1}^t), \tag{6}$$

where $\sigma_x\equiv\sigma_\parallel$ and $\sigma_y\equiv\sigma_\perp$. It follows that the excess pressure Π_x contains a background contribution, $-2\sigma_\perp/L_y$, that is independent of L_x. At fixed L_y the strength and sign of this term are determined by $\sigma_\perp$, that depends in turn on the nature of the confining walls and on the period of the lamellar phase [6].

At $L_x=L_N^t$ the number of layers in the pore increases from $N-1\to N$. Therefore, $(L_x-L_N)^2$ and $B_l/2L_N$ in Eq. (6) may be written as

$$L_x-L_N=L_x-\left[L_{N_0}+\lambda\sum_{N=N_0+1}\theta(L_x-L_N^t)\right], \tag{7}$$

$$\frac{B_l}{2L_N}=\frac{B_l}{2}\left[\frac{1}{L_{N_0}}+\sum_{N=N_0+1}\left(\frac{1}{L_N}-\frac{1}{L_{N-1}}\right)\theta(L_x-L_N^t)\right], \tag{8}$$

where we assumed that the system is elastic for $N>N_0$, i.e., Eq. (6) is valid for $L_x>L_{N_0}$. Note that the unit step functions $\theta(L_x-L_N^t)$ in the previous equations yield δ functions $\Sigma_{N>N_0}a_N\delta(L_x-L_N^t)$ in the excess pressure. Experimentally these δ functions correspond to instabilities at the transitions $N-1\to N$ that take place when $L_x=L_N^t$.

Let us consider square base pores and deformations that conserve this symmetry. The excess pressure (5) for the confined lamellar phase is then

$$\Pi(L)=-\frac{1}{L}(\sigma_\parallel+\sigma_\perp)-\frac{B_l(L-L_N)}{2L_N}\left(1+\frac{L-L_N}{2L}\right) \qquad (L_N^t<L<L_{N+1}^t). \tag{9}$$

For $L_N\gg\lambda$ the above may be expanded as

$$\Pi(L)+\frac{1}{L}(\sigma_\parallel+\sigma_\perp)=-\frac{B_l}{2}x-\frac{B_l}{4}x^2+\frac{B_l}{4}x^3+O(x^4), \qquad (L_N^t<L<L_{N+1}^t), \tag{10}$$

where $x=(L-L_N)/L_N$.

B. Quasionion structure

In square base pores with identical walls the directions x and y are equivalent. Since lamellas tend to be parallel to strongly hydrophilic walls we consider the mechanical properties of the stable or metastable structures, with lamellas

parallel to neighboring walls with domain walls, along the diagonals of the square, separating perpendicularly aligned lamellas [see Fig. 1(b)].

The domain walls meet at the center of the square. We refer to this structure as ''quasionion.'' The domain walls are associated with additional contributions to Ω_{ex}, which are present even in the absence of compression or expansion of the layers (i.e., when $L=L_N$). For a system with $L=L_N$, we assume for the elastic quasionion excess grand potential

$$\Omega_{ex}(L_N)/L_z=4L_N\sigma_{\|}+2\sqrt{2}L_N\gamma+\delta, \tag{11}$$

where γ is the surface tension associated with the domain walls and δ the line tension along the axis of the pore where the domain walls intersect. If, in addition, we assume that the elastic contribution $\Omega_{el}/L_z=B_o(L-L_N)^2L/2L_N$ is also present, we obtain for the quasionion structure

$$\Pi(L)=-\frac{1}{L}(2\sigma_{\|}+\sqrt{2}\gamma)-\frac{B_o(L-L_N)}{2L_N}\left(1+\frac{L-L_N}{2L}\right)$$

$$(L_N^t<L<L_{N+1}^t), \tag{12}$$

where B_o is the modulus of elasticity of the onion structure. Instabilities at $L=L_N^t$, associated with terms in $\Pi(L)$ of the form $\Sigma_{N>N_0}b_N\delta(L-L_N^t)$, are also present.

The quasionion structure bears some resemblance to cylindrical membranes separating concentric oil- and water-rich layers in cylindrical pores. The elastic properties of the latter may be determined from the Helfrich model [12], with an excess pressure given by

$$\Pi_H(R)=-\frac{1}{R}\left(\alpha+\frac{\kappa}{2R}\right), \tag{13}$$

where α is related to the surface tension and κ is the bending rigidity. Note that the two geometries exhibit a similar dependence of Π on L [Eq. (12)] and R [Eq. (13)].

For rectangular base pores we expect stable or metastable structures of the type shown in Fig. 1(c). In the absence of stress, i.e., for $L_x=L_N$, and $L_x<L_y$ we assume

$$\Omega_{ex}(L_x,L_y)/L_z=2(L_x+L_y)\sigma_{\|}+2\sqrt{2}L_x\gamma+\delta. \tag{14}$$

Note that the stability or metastability of the lamellar or quasionion structures is determined by the minimum of Ω_{ex}, which depends on $\sigma_{\|}$, $\sigma_{\perp}$, γ, δ, B_l, B_o, and λ. Assuming that the above description is correct, we need to determine the values of these parameters to establish the stability of each structure. In addition, the stability of other, more complex structures cannot be ruled out. Consequently, the phenomenological theory is not sufficient to describe lamellar phases confined in pores with rectangular bases. In the following, we will determine the stable structures in long pores for different types of walls, by explicit calculations based on the CHS model. We will also check, for this model, the validity of the phenomenological description for the mechanical properties of the structures discussed in this section.

III. MODEL

The CHS model [11] is a generic model for a mixture of polar and nonpolar components and amphiphiles. In general, M orientations of amphiphiles are considered. On a simple cubic lattice every lattice site $\mathbf{x}$ is occupied by either oil, water, or an amphiphile in an orientation $\hat{\boldsymbol{\omega}}_m$, $m=1,\ldots,M$, and thus there are $2+M$ microscopic states $\hat{\rho}_i(\mathbf{x})$ at each $\mathbf{x}$. $\hat{\rho}_i(\mathbf{x})=1(0)$ if the site $\mathbf{x}$ is (is not) occupied by the state i, where $i=1,2,\ldots,2+M$ denotes water, oil and surfactant in different orientations, respectively. In the case of close-packing and oil-water symmetry only one chemical potential is relevant, namely $\mu=\mu_1-\mu_s=\mu_2-\mu_s$, with $\mu_s=\mu_i$ for $i>2$. The Hamiltonian in the presence of external fields $h_i(\mathbf{x})$ is written as

$$H=\frac{1}{2}\sum_{\mathbf{x}\neq\mathbf{x}'}\sum_{i,j}\hat{\rho}_i(\mathbf{x})\mathrm{U}_{ij}(\mathbf{x}-\mathbf{x}')\hat{\rho}_j(\mathbf{x}')+\sum_{\mathbf{x}}\sum_i h_i(\mathbf{x})\hat{\rho}_i(\mathbf{x})$$

$$-\mu\sum_{\mathbf{x}}(\hat{\rho}_1(\mathbf{x})+\hat{\rho}_2(\mathbf{x})). \tag{15}$$

The lattice constant $a\equiv 1$ is identified with the size of the amphiphiles (~ 2 nm). Nearest-neighbor interactions are assumed and $U_{ij}(\mathbf{x}-\mathbf{x}')$ vanishes for $|\mathbf{x}-\mathbf{x}'|\neq 1$. In the case of oil-water symmetry the water-water and oil-oil interactions have the same strength $-b$, and the water-oil interaction energy is set to zero. The interaction between an amphiphile in an orientation $\hat{\boldsymbol{\omega}}$ at $\mathbf{x}$ and a water molecule at $\mathbf{x}'$ is proportional to the scalar product $\hat{\boldsymbol{\omega}}\cdot\Delta\mathbf{x}$, where $\Delta\mathbf{x}=\mathbf{x}-\mathbf{x}'$. The same strength c and the opposite sign is assumed for the interaction between an amphiphile in orientation $\hat{\omega}$ at $\mathbf{x}$ and an oil molecule at $\mathbf{x}'$, i.e., opposite orientations of amphiphiles are preferred by the water and the oil, as in real systems. Two amphiphiles with orientations $\hat{\boldsymbol{\omega}}$ and $\hat{\boldsymbol{\omega}}'$ at $\mathbf{x}$ and $\mathbf{x}'$, respectively, contribute $-g(\hat{\boldsymbol{\omega}}\times\Delta\mathbf{x})\cdot(\hat{\boldsymbol{\omega}}'\times\Delta\mathbf{x})$ to the system energy (when $|\Delta\mathbf{x}|=1$). g describes the tendency for avoiding the unfavorable contacts between the polar and nonpolar parts of two amphiphiles and supports formation of planar monolayers with amphiphiles parallel to each other and perpendicular to the plane of the monolayer. Formal expressions for $\mathrm{U}_{ij}(\mathbf{x}-\mathbf{x}')$ can be found in Ref. [4].

We assume now that $L_z\to\infty$ and that the structure in the pore is translationally invariant in the z direction. In this case the projection of the orientation of the amphiphiles onto the (x,y) plane is sufficient to describe the structure of the system. Density distributions and excess pressures in the pore can thus be calculated in the 2D version of the CHS model, where $\hat{\boldsymbol{\omega}}$ lies in the (x,y) plane. Following Ref. [6] we project $\hat{\boldsymbol{\omega}}$ onto the unit lattice vectors in the (x,y) plane, $\hat{\mathbf{e}}_i$, $i=1,2$ and we distinguish four different states, that may be described by $\pm\hat{\mathbf{e}}_i$, $i=1,2$. We consider three types of boundary conditions: (i) The walls are water-covered or strongly hydrophilic; the interactions with boundary sites are the same as with the water-occupied sites in the bulk; (ii) the walls are neutral–the interaction with the the boundary sites is zero; and finally (iii) one pair of parallel walls is

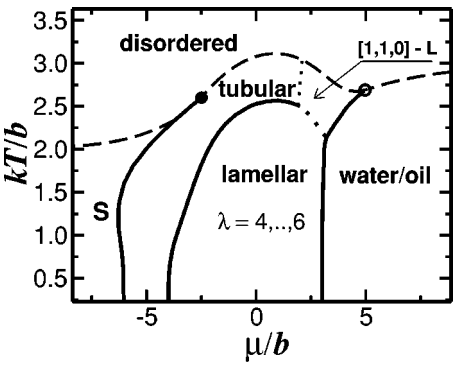

FIG. 2. $(kT/b,\mu/b)$ phase diagram for the six-state model with four orientations of surfactant molecules. Here k is Boltzmann's constant, T is the temperature, μ is the difference between the chemical potential of water and surfactant (oil-water symmetry is assumed), and b is the parameter controlling the water-water interaction. The coupling constants are $c/b=2.5, g/b=1$. c measures the interaction of the water (oil) with the surfactant head or tail group and g is the surfactant-surfactant spinlike coupling constant. S denotes the region where the surfactant-rich smectic phase is stable. Solid and dashed lines represent first- and second-order phase boundaries, respectively, as obtained in the MF approximation. Lamellar phases oriented in (1,1,0) directions are stable in a region close to the Lifshitz point (open circle).

hydrophilic and the other is neutral. It is straightforward to write down the expressions for the external fields $h_i(\mathbf{x})$ corresponding to these boundary conditions.

The structure of the stable configuration is obtained by minimizing the mean-field grand potential

$$\Omega^{MF}(T,\mu,L)=\sum_{\mathbf{x}}\sum_{i}\rho_i(\mathbf{x})\Big\{kT\ln[\rho_i(\mathbf{x})]+\frac{1}{2}\phi_i(\mathbf{x})+h_i(\mathbf{x})-\mu(\delta_{i1}+\delta_{i2})\Big\}. \tag{16}$$

Here $\phi_i(\mathbf{x})=\Sigma_{\mathbf{x}'}\Sigma_j U_{ij}(\mathbf{x}-\mathbf{x}')\rho_j(\mathbf{x}')$ is the mean field (MF) acting on species i at site $\mathbf{x}$ and $\rho_i(\mathbf{x})$ is the MF average of $\hat{\rho}_i(\mathbf{x})$. We minimize Eq. (16) numerically by solving a set of self-consistent algebraic equations [4] for the one-point distribution functions $\rho_i(\mathbf{x})$.

The MF bulk phase diagram of the 2D model was found in Ref. [6]. In Fig. 2 the $(kT/b,\mu/b)$ phase diagram is shown for fixed interactions $c/b=2.5$ and $g/b=1$. The stable phases are: microemulsion, oil-rich, water-rich, a phase with 2D density oscillations (tubular phase), surfactant-rich phase with smectic order and finally lamellar phases. In continuum models all orientations of the bulk lamellas are equivalent but on a lattice this rotational symmetry is broken. Therefore, the lattice lamellar phases are characterized by the density profiles in the direction of the oscillations and in addition by the orientation of the normal to the layers $\hat{\mathbf{n}}$. In the CHS model the short period phases, with $\lambda\leqslant 6$, are characterized by $\hat{\mathbf{n}}=(1,0,0)$ or $\hat{\mathbf{n}}=(0,1,0)$, or $\hat{\mathbf{n}}=(0,0,1)$, while swollen phases, $\lambda>6$, have $\hat{\mathbf{n}}=(\pm 1,\pm 1,0)$, $\hat{\mathbf{n}}=(\pm 1,0,\pm 1)$, etc. Walls that are perpendicular to the principal directions of the lattice are compatible with the orientation of lamellas in the short period but not in swollen lamellar phases. In real systems, lamellas are parallel to the strongly hydrophilic walls, and to model this in the swollen regime one has to consider walls that are perpendicular to $\hat{\mathbf{n}}=(\pm 1,\pm 1,0)$ etc. This geometry is somewhat more complicated and in this study we restrict ourselves to short period lamellar phases, $\lambda\leqslant 6$, which are stable in the middle of the phase diagram.

IV. RESULTS

The stable configuration in the pore is the global minimum of Ω^{MF} Eq. (16). We find the local minima numerically by solving the self-consistent set of equations for the densities [4]. As initial configurations we use 4 classes of density distributions corresponding to lamellar, tubular, 2D quasionion and 2D quasicigar structures. The quasicigar structure could be imaging as follows: near the walls the surfactant monolayer followed by the oil-rich layer is formed, and this outer shell encloses a lamellar structure, as is shown in Fig. 10. Cross section of this structure resembles parallel cigars and we term this phase ''quasicigar'' to distinguish it from the lamellar phase shown in Fig. 1(a).

We consider a single system, specified by $c/b=2.5$ and $g/b=1$. The corresponding $(kT/b,\mu/b)$ phase diagram is shown in Fig. 2. In most cases we choose a thermodynamic state corresponding to a stable period-6 lamellar phase, far from coexistence with the tubular phase, and study the effects of different boundary conditions and pore geometries (square and rectangular bases).

On the lattice L_x does not change continuously, and the derivative $\partial/\partial L_x$ is replaced by the lattice first-order difference operator. The excess pressure (3) is thus obtained by calculating the difference in Ω_{ex} for two consecutive values of L_x. Also, the transition $N\rightarrow N+1$ occurs between two values of L_x that differ by 1 and thus the unit step functions in Ω_{ex} lead to Kronecker δ functions in the excess pressure on the lattice.

The numerical values Ω_{ex}, Π_x, and Π are compared with the phenomenological predictions of the Sec. II. In all cases we insert into the phenomenological expressions the surface tensions determined by independent calculations. Namely, the wall-fluid surface energy is calculated from $\Omega_{ex}(L_x)/L_yL_z$ with $L_y, L_z\rightarrow\infty$, and $L_x=L_N$ sufficiently large, so that $\Omega_{ex}(L_x)/L_yL_z$ is independent of L_x.

A. Free boundary conditions

If $(kT/b,\mu/b)$ is far from the phase boundary with the tubular phase, *a long pore with neutral walls favors the lamellar structure*. At $kT/b=2.1, \mu/b=3.1$ and for neutral walls, the surface tensions were found to be $\sigma_{\parallel}=0.263b/a^2$ and $\sigma_{\perp}=0.244b/a^2$. Note that $\sigma_{\parallel}>\sigma_{\perp}$; neutral walls favor perpendicular orientation of short period lamellar phases [6]. The reason is the translational entropy loss in the parallel orientation, when the oil- or water-rich layer is pinned at the wall [6]. In the rectangular base pore the lamellas are parallel to the walls with the shortest separation.

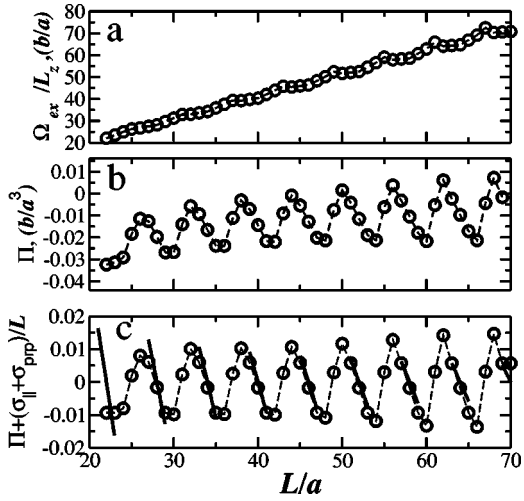

FIG. 3. (a) Surface excess grand potential Ω_{ex}/L_z, (b) the excess pressure $\Pi=-(1/2L_zL)\partial\Omega_{ex}/\partial L$, (c) $\Pi(L)+(\sigma_\parallel+\sigma_\perp)/L$ [see Eqs. (9) and (10)] for the square base pore with side L and height L_z as functions of L. The walls are neutral (surface fields $h_i=0$). The solid lines in (c) are given by the first term on the rhs of Eq. (10) for L such that $|L-L_N|\leqslant 1$. The surface tensions are $\sigma_\parallel=0.263b/a^2$ and $\sigma_\perp=0.244b/a^2$. The optimal value of the fitting parameter B_l is $B_l=0.350kT/a^3$. The thermodynamic variables $kT/b=2.1, \mu/b=3.1$ and material constants $c/b=2.5, g/b=1$ correspond to a stable lamellar phase with period $\lambda=6$. For any value of L the square base pore favors the lamellar structure. Lengths are measured in units of the lattice constant a, and b is the water-water interaction energy.

Numerical results for $\Omega_{ex}(L)/L_2$ and $\Pi(L)$ of the square base pore are shown in Fig. 3. In order to compare $\Pi(L)$ with Eq. (9) for elastic systems, we plot $\Pi(L)+(\sigma_\parallel+\sigma_\perp)/L$ in Fig. 3(c) [see Eq. (10)]. B_l is used as a fitting parameter. Since Eq. (10) is an approximation valid for small deformations $x=(L-L_N)/L_N$, and deviations are expected for large x, we used three values of x for the fit, namely, $x=-1/L_N, 0, 1/L_N$. The best fit corresponds to $B_l=0.350kT/a^3$. Note that in the present work we do not study the swollen phases, which are much softer. For example, B_l is two orders of magnitude smaller for swollen lamellar phases, with $\lambda\approx 15$ (in units of a) in the CHS model [4]. The high stiffness of the short period lamellar phases of the CHS model is consistent with the results for a stack of parallel elastic membranes [12], where $B\propto\lambda/(\lambda-2a)^4$. The wall-fluid surface tensions are also different for swollen phases [6]; in particular, $\sigma_\parallel<\sigma_\perp$. Therefore the above results are restricted to short period, stiff lamellar phases, and may not hold for swollen phases.

In Fig. 4 we plot $\Omega_{ex}(L)$ and $\Pi(L)$ at $(kT/b, \mu/b)$ close to the lamellar-tubular phase boundary. In this case a tubular phase is formed inside the pore. This is the analog of capillary condensation. The tubular phase is compatible with the simple cubic lattice. In real systems capillary condensation of a hexagonal phase is expected close to the phase boundary.

B. Mixed boundary conditions

We assume that two parallel walls are hydrophilic while the other two are neutral. These boundary conditions are relevant for experiments, where a small droplet is confined between parallel hydrophilic plates, and free surfaces develop in a direction perpendicular to the plates. We find a stable lamellar phase with *lamellas parallel to the hydrophilic walls*. Parallel orientation of the lamellas is strongly favored by the hydrophilic walls; the surface tension is $\sigma_\parallel=-0.588b/a^2$. $\Omega_{ex}(L_x)/L_yL_z$ is shown in Fig. 5(b) for $L_x\ll L_y$, deep into the stability region of the $\lambda=6$ lamellar phase. The surface tension $\sigma_\perp$ is positive for neutral walls (in our case $\sigma_\perp=0.244b/a^2$) and thus Ω_{ex}/L_yL_z increases monotonically as a function of L_x. The excess pressure $\Pi(L_x)$ has an attractive background in addition to the oscil-

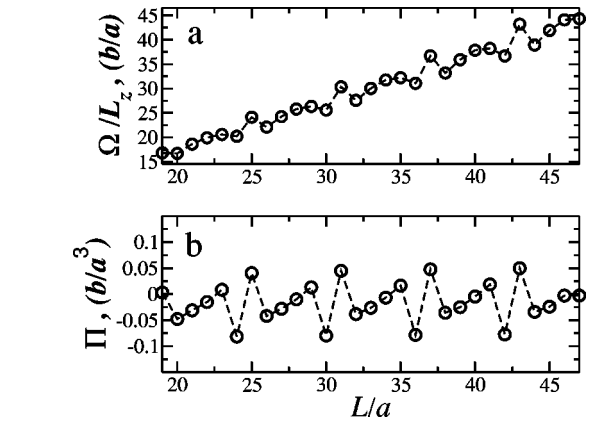

FIG. 4. (a) Surface excess grand potential Ω_{ex}/L_z and (b) the excess pressure Π for the square base pore with side L and height L_z, as functions of L. The walls are neutral (surface fields $h_i=0$). The thermodynamic variables $kT/b=2.56$, $\mu/b=1.0$ and material constants $c/b=2.5$, $g/b=1$ correspond to a stable lamellar phase with period $\lambda=4$. For any value of L the square pore favors the tubular phase. Lengths are measured in units of the lattice constant a, and b is the water-water interaction strength.

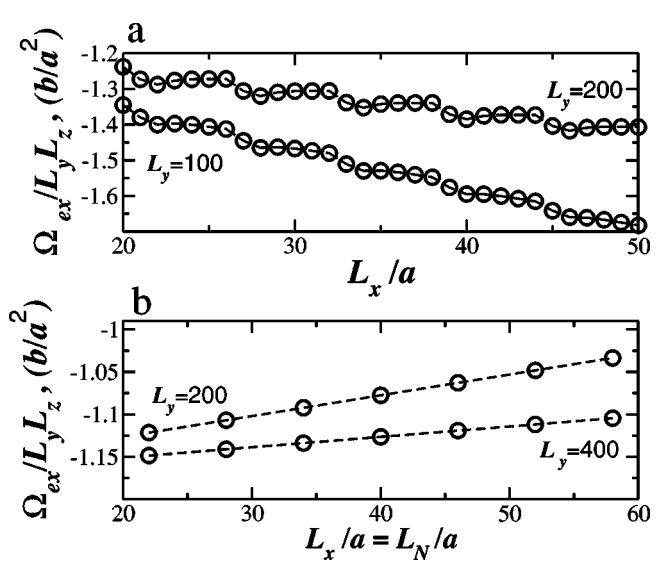

FIG. 5. Rectangular base pore, $1\leqslant x\leqslant L_x$, $1\leqslant y\leqslant L_y$, and $L_x\ll L_y$. Ω_{ex}/L_yL_z as a function of L_x for fixed L_y is shown for (a) hydrophilic walls; (b) two hydrophylic walls at a distance L_x and the other two neutral. $kT/b=2.1$, $\mu/b=3.1$, $c/b=2.5$, $g/b=1$.

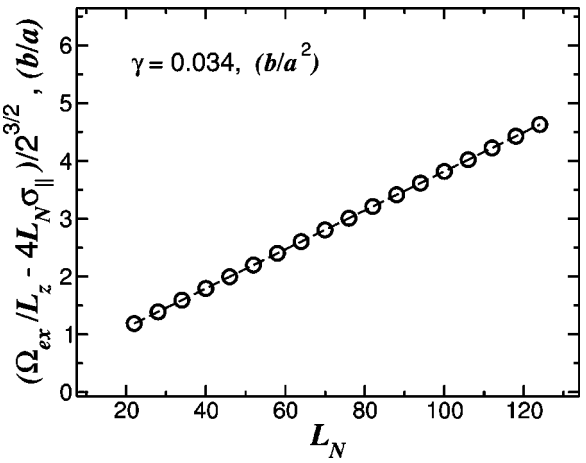

FIG. 6. $(\Omega_{ex}/L_z-4L_N\sigma_\parallel)/2\sqrt{2}$ (open circles) as a function of the side of the square base $L=L_N$ that is commensurate with $\lambda/a=6$. The dashed line is a linear interpolation with slope $\gamma=0.034b/a^2$, yielding the energy density of the domain wall between two lamellar domains, with density oscillations in the (1,0,0) and (0,1,0) directions, respectively. The energy scale is set by b, the interaction energy between two neighboring water-water (or oil-oil) molecules.

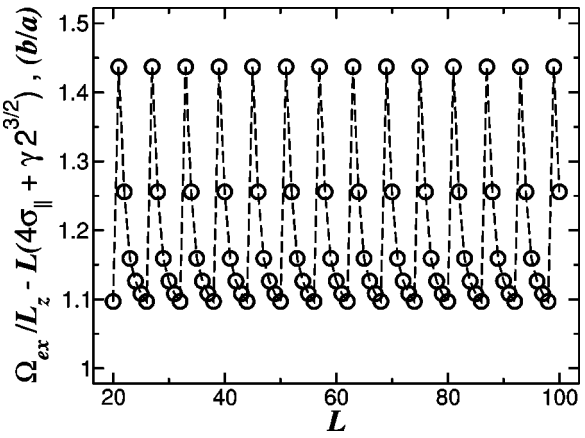

FIG. 7. $\Omega_{ex}/L_z-(4L\sigma_\parallel+2\sqrt{2}L\gamma)$ as a function of the side L of the square base pore of height L_z, for $c/b=2.1$, $g/b=1$, $kT/b=2.1$, and $\mu/b=3.1$.

lations resulting from the elastic contribution to Ω_{ex}. If $2\sigma_\perp/L_y>B\lambda/2L_N$ then $\Pi(L_x)<0$ for all L_x. Similar behavior (oscillations superimposed on an attractive background) has been observed experimentally in surface force aparatus measurements [9,13,14].

C. Hydrophilic walls

If the walls are water covered, or strongly hydrophilic, and the lamellar phase with $\lambda/a=6$ is deeply stable, then *the quasionion structure is favored by the pore for all pore sizes.* In Fig. 6 we plot $[\Omega_{ex}(L_N)/L_z-4L_N\sigma_\parallel]/2\sqrt{2}$ as a function of the L_N for the square base pore and $kT/b=2.1,\mu/b=3.1$. The numerical values are in good agreement with the linear behavior predicted by Eq. (11). The slope of the straight line gives the domain-wall free-energy density, $\gamma=0.034b/a^2=0.016kT/a^2$. Note that this domain-wall energy is low compared with kT/a^2 meaning that deformations of the structure controlled by these energies are thermally excited. In fact a lamellar phase with a large number of this type of defects was observed in systems of copolymers Refs. [15–20]. In our system $\gamma\ll|\sigma_\parallel|$, the latter being negative, $\sigma_\parallel=-0.588b/a^2$. Both, the low value of γ and the large, negative value of $\sigma_\parallel$ contribute to the stability of the quasionion structure in pores with hydrophilic walls.

In Fig. 7 we plot $\Omega_{ex}/L_z-(4L\sigma_\parallel+2\sqrt{2}L\gamma)$ as a function of the L, in order to study the contribution to the free energy associated with the incompatibility between L and λ. For an elastic response to compression or expansion, the above quantity should have the form postulated above Eq. (12),

$$\Omega_{el}/L_z=\frac{B_o(L-L_N)^2}{2}\left(1+\frac{L-L_N}{L_N}\right), \qquad (17)$$

i.e., it should be parabolic around $L=L_N$. In Fig. 7 the symbols represent numerical values. Note the large deviations from elastic behavior. In an elastic system, such as a stack of elastic membranes, the width of N confined lamellas is smaller or larger than in bulk when the system with $L=L_N$ is compressed or expanded, respectively. However, the deformations of the onion structure are quite different. In Fig. 8(a) we plot the expanded structure before the insertion of a new layer, and in Fig. 8(b) the compressed structure, after the insertion of that layer. The deformation of the structure in both cases is localized in the central region of the pore, while the outer layers are undeformed. It turns out that swelling or shrinking the core alone (i.e., the central tube) costs a lower free energy than a uniform change of the period over the whole system. In Fig. 9 we plot the corresponding excess pressure. Note the discontinuities that occur when the new central tube is inserted into the system. The excess pressure in this case is similar to the excess pressure in a cylindrical pore given by Eq. (13) and shown in Fig. 9 as a solid line, for $\alpha=-1.143b/a^2$ and $\kappa=1.230b/a$. Note that this result applies to short period, stiff lamellar phases; it is unclear if the swollen phases respond in a similar fashion or if they re-

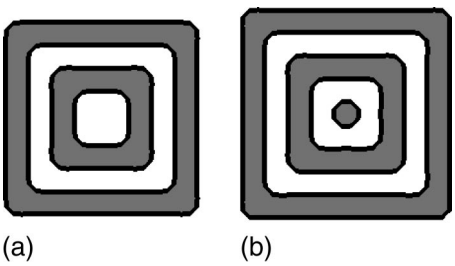

FIG. 8. Cross section of the pore at fixed $z[(x,y)$ plane] for $kT/b=2.1$, $\mu/b=3.1$, $c/b=2.5$, $g/b=1$ and hydrophilic walls. Shaded regions represent the oil-rich domains and white regions represent the water-rich domains. Thick lines represent the local interfaces $\rho_1(x,y)-\rho_2(x,y)=0$, where ρ_1,ρ_2 are the MF averaged densities of water and oil, respectively. (a) $L=26$ and (b) $L=28$ (in units of the lattice constant a).

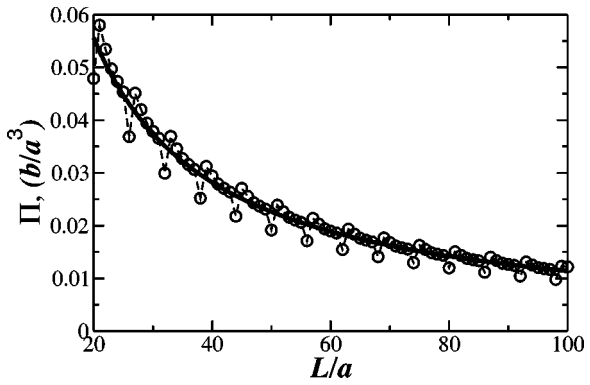

FIG. 9. Excess pressure $\Pi=-(1/2L_zL)\partial\Omega_{ex}/\partial L$ for a pore with a square base of side L and height L_z, as a function of L. The walls of the pore are hydrophilic. The thermodynamic variables $kT/b=2.1, \mu/b=3.1$ and the material constants $c/b=2.1$, $g/b=1$ correspond to a stable lamellar phase with period $\lambda=6$. For any value of L, the square pore favors the 2D onion configuration. The solid line is the excess pressure in a cylindrical pore given by Eq. (13) for $\alpha=-1.143b/a^2$ and $\kappa=1.230b/a$. The leading contribution to Π scales with L as $-(2\sigma_{\|}+\sqrt{2}\gamma)L^{-1}$ [see Eq. (12)], and from the previous results one has $-(2\sigma_{\|}+\sqrt{2}\gamma)=1.128b/a^2$. Lengths are measured in units of the lattice constant a.

spond elastically, i.e., by shrinking or swelling the layers uniformly over the whole system. Finally, note that the leading behavior of Π is determined by the surface tension, rather than by the elastic or inelastic response to compression and expansion.

For the rectangular base pore we confirm the stability of the structure shown in Fig. 1(c). In this case the lamellas are parallel to the nearest walls, and since $\sigma_{\|}=-0.588$, a strong repulsive background appears in the excess pressure. In Fig. 5(a) $\Omega_{ex}(L_x)$ is shown at $kT/b=2.1$, $\mu/b=3.1$, and two values of L_y.

The quasicigar phase mentioned at the beginning of this section is not stable for the period-6 lamellar phase, for any type of the boundary conditions considered here. However, when $kT/b, \mu/b$ correspond to a stable period-4 lamellar phase and the pore size $L_x=L_y=L$ is commensurate with the period, the quasicigar phase, shown in Fig. 10, becomes stable.

Finally, we describe the metastable structures that may form in long pores for soft, large period lamellar phases. Consider a pore with surface normals in the direction of the unit lattice vectors $\hat{\mathbf{x}},\hat{\mathbf{y}}$, respectively. The direction of the density oscillations in the stable lamellar phase, $(\hat{\mathbf{x}}+\hat{\mathbf{y}})/\sqrt{2}$, is at 45° with the normals. In this case the lowest value of Ω_{ex} corresponds to the structure shown in Fig. 11. As already noted, hydrophilic walls favor a parallel orientation of the lamellas and thus this structure is not stable in real (continuum) systems but it could be metastable. If a long capillary is inserted into a bulk lamellar phase, with the walls at 45° with the lamellas, similar structures may form at short or intermediate time scales, if the viscosity of the system is high.

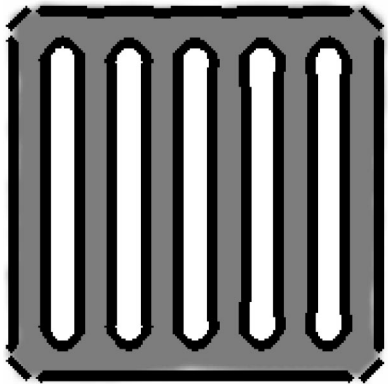

FIG. 10. Cross section of the pore at fixed $z[(x,y)$ plane] for $kT/b=2.55$, $\mu/b=1$, $c/b=2.5$, $g/b=1$ and hydrophilic walls. Shaded regions represent the oil-rich domains and white regions represent the water-rich domains. Thick lines represent the local interfaces $\rho_1(x,y)-\rho_2(x,y)=0$, where ρ_1,ρ_2 are the MF averaged densities of water and oil, respectively. $L=23$ (in units of the lattice constant a).

V. SUMMARY

Lamellar phases confined to long pores with a rectangular base are studied within the 2D CHS lattice model of microemulsions. We restrict ourselves to that part of phase diagram where lamellar phases oriented in (1,0,0) or (0,1,0) directions are stable. These are short period stiff lamellar phases. However, the numerical excess pressures obtained for different boundary conditions and pore geometries are in good agreement with those predicted for elastic systems.

For square pores with hydrophilic walls, the 2D onion structure is stable in the pore. The excess pressure in this case is positive and falls off as $\sim L^{-1}$, where L is the pore size. Square pores with neutral walls stabilize the tubular phase if the bulk lamellar phase is close to that phase boundary; otherwise the lamellar phase is stable. When the tubular phase is stabilized in the square base pore the excess pressure

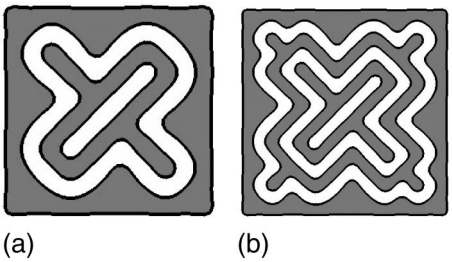

FIG. 11. Cross section of the pore at fixed $z[(x,y)$ plane] for $kT/b=2.5$, $\mu/b=4.01$, $c/b=2.5$, $g/b=1$ and hydrophilic walls. For this set of thermodynamic variables a bulk lamellar phase with density oscillations in the (1,1,0) direction is stable. The walls are normal to the unit lattice vectors. Shaded regions represent the oil-rich domains and white regions represent the water-rich domains. Thick lines represent the local interfaces $\rho_1(x,y)-\rho_2(x,y)=0$ where ρ_1,ρ_2 are the MF averaged densities of water and oil, respectively. (a) $L=40$ and (b) $L=60$ (in units of the lattice constant a).

$\Pi(L)$ oscillates about const<0. When the lamellar phase is stabilized in the pore, the excess pressure $\Pi(L)$ is negative and oscillates about L^{-1}.

The results obtained for the rectangular geometry may be compared with those calculated for the slit geometry [4]. In the slit the solvation force oscillates around zero as a function of the distance between the walls. By contrast, for fixed L_y $(L_y>L_x)$, the surface contribution associated with the L_y walls shifts the excess pressure $\Pi(L_y)$ above (hydrophilic L_y walls) or below (neutral L_y walls) zero.

ACKNOWLEDGMENTS

This research was supported in part by the KBN Grant No. 3T09A 073 16 (A.C.) and by the Fundação para a Ciência e a Tecnologia (FCT) through Grant No. SFRH/BPD/1599/2000 (M.T.).

[1] M. W. Matsen and F. S. Bates, Macromolecules **29**, 1091 (1996).
[2] M. Laradji, A. C. Shi, R. C. Desai, and J. Noolandi, Phys. Rev. Lett. **78**, 2577 (1997).
[3] G. Gompper and M. Schick, *Self-Assembling Amphiphilic Systems*, 1st ed., Phase Transitions and Critical Phenomena Vol. 16 (Academic Press, New York, 1994).
[4] M. Tasinkevych and A. Ciach, Phys. Rev. E **60**, 7088 (1999).
[5] V. Babin, A. Ciach, and M. Tasinkevych, J. Chem. Phys. **114**, 9585 (2001).
[6] M. Tasinkevych and A. Ciach, J. Chem. Phys. **115**, 8705 (2001).
[7] F. Schmid and M. Schick, Phys. Rev. E **48**, 1882 (1993).
[8] G. Gompper and M. Kraus, Phys. Rev. E **47**, 4301 (1993).
[9] P. Richetti, P. Kékicheff, J. L. Parker, and B. W. Ninham, Nature (London) **346**, 252 (1990).
[10] D. A. Antelmi and P. Kékicheff, J. Phys. Chem. B **101**, 8169 (1997).
[11] A. Ciach, J. S. Høye, and G. Stell, J. Phys. A **21**, L777 (1988).
[12] W. Helfrich, Z. Naturforsch. A **33A**, 305 (1978).
[13] P. Kékicheff, P. Richetti, and H. Christenson, Langmuir **7**, 1874 (1991).
[14] E. Freyssingeas, D. Antelmi, P. Kékicheff, P. Richetti, and A.-M. Bellocq, Eur. Phys. J. B **9**, 123 (1999).
[15] D. G. Walton, G. J. Kellogg, A. M. Mayes, P. Lambooy, and T. P. Russel, Macromolecules **27**, 6225 (1994).
[16] P. Mansky, E. Huang, Y. Liu, T. P. Russel, and C. Hawker, Science **275**, 1458 (1997).
[17] G. Brown and A. Chakrabarti, J. Chem. Phys. **102**, 1440 (1995).
[18] G. J. Kellogg *et al.*, Phys. Rev. Lett. **76**, 2503 (1996).
[19] G. T. Pickett and A. C. Balazs, Macromolecules **30**, 3097 (1997).
[20] M. Kikuchi, J. Chem. Phys. **101**, 3367 (1994).